Quantitative and Qualitative Analyses of Biodistribution and PET Image Quality of a Novel Radiohybrid PSMA, ^{18}F-rhPSMA-7, in Patients with Prostate Cancer

So Won Oh[1,2], Alexander Wurzer[3], Eugene J. Teoh[4], Sohee Oh[5], Thomas Langbein[1], Markus Krönke[1], Michael Herz[1], Saskia Kropf[6], Hans-Jürgen Wester[3], Wolfgang A. Weber[1], and Matthias Eiber[1]

[1]Department of Nuclear Medicine, School of Medicine, Klinikum rechts der Isar, Technical University of Munich, Munich, Germany; [2]Department of Nuclear Medicine, Seoul National University Boramae Medical Center, Seoul, Korea; [3]Technical University of Munich, Garching, Germany; [4]Department of Radiology and Nuclear Medicine, Oxford University Hospitals NHS Foundation Trust, Oxford, United Kingdom; [5]Department of Biostatistics, Seoul National University Boramae Medical Center, Seoul, Korea; and [6]Scintomics GmbH, Fuenstenfeldbruck, Germany

Radiohybrid PSMA (rhPSMA) ligands, a new class of theranostic prostate-specific membrane antigen (PSMA)–targeting agents, feature fast ^{18}F synthesis and utility for labeling with radiometals. Here, we assessed the biodistribution and image quality of ^{18}F-rhPSMA-7 to determine the best imaging time point for patients with prostate cancer. **Methods:** In total, 202 prostate cancer patients who underwent a clinically indicated ^{18}F-rhPSMA-7 PET/CT were retrospectively analyzed, and 12 groups based on the administered activity and uptake time of PET scanning were created: 3 administered activities (low, 222–296 MBq; moderate, 297–370 MBq; and high, 371–444 MBq) and 4 uptake time points (short, 50–70 min; intermediate, 71–90 min; long, 91–110 min; and extra long, ≥111 min). For quantitative analyses, SUV_{mean} and organ- or tumor-to-background ratio were determined for background, healthy organs, and 3 representative tumor lesions. Qualitative analyses assessed overall image quality, nonspecific blood-pool activity, and background uptake in bone or marrow using 3- or 4-point scales. **Results:** In quantitative analyses, SUV_{mean} showed a significant decrease in the blood pool and lungs and an increase in the kidneys, bladder, and bones as the uptake time increased. SUV_{mean} showed a trend to increase in the blood pool and bones as the administered activity increased. However, no significant differences were found in 377 tumor lesions with respect to the administered activity or uptake time. In qualitative analyses, the overall image quality was stable along with the uptake time, but the proportion rated to have good image quality decreased as the administered activity increased. All other qualitative image parameters showed no significant differences for the administered activities, but they showed significant trends with increasing uptake time: less nonspecific blood activity, more frequent background uptake in the bone marrow, and increased negative impact on clinical decision making. **Conclusion:** The biodistribution of ^{18}F-rhPSMA-7 was similar to that of established PSMA ligands, and tumor uptake of ^{18}F-rhPSMA-7 was stable across the administered activities and uptake times. An early imaging time point (50–70 min) is recommended for ^{18}F-rhPSMA-7 PET/CT to achieve the highest overall image quality.

Key Words: ^{18}F-rhPSMA-7; biodistribution; PET; prostate cancer; uptake time

J Nucl Med 2020; 61:702–709
DOI: 10.2967/jnumed.119.234609

Prostate-specific membrane antigen (PSMA)–targeting ligands have been extensively investigated for molecular imaging and radioligand therapy of prostate cancer. Among these ligands, ^{68}Ga labeled with Glu-NH-CO-NH-Lys-(Ahx) (^{68}Ga-PSMA-11) is most widely used in clinical settings. However, ^{68}Ga-PSMA-11 is rapidly excreted via the urinary tract, resulting in intense accumulation in the urinary bladder.

^{18}F-based PET is preferred to ^{68}Ga-based PET because of ease of production as well as better handling and image resolution. The shorter half-life of ^{68}Ga often limits clinical availability compared with ^{18}F, because distribution of ^{68}Ga-based PET agents from a central facility to local imaging centers is infeasible. The limited size of a ^{68}Ge/^{68}Ga generator results in a quantity of activity suitable for only 2–4 patients. Moreover, operating the ^{68}Ge/^{68}Ga generator becomes less economical in local imaging centers because of its high price and relatively low productivity. Lastly, ^{68}Ga has a higher positron energy than ^{18}F, which reduces the theoretic maximum spatial resolution (*1*). Consequently, the unique characteristics of ^{18}F, which include a relatively longer half-life and shorter positron energy, and the possibility of its large-scale production from cyclotrons have encouraged the development of ^{18}F-based PSMA ligands for clinical prostate cancer imaging.

Several research groups have focused on the development of ^{18}F-based PSMA ligands. The first of its generation, *N*-[*N*-[(*S*)-1,3-dicarboxypropyl]carbamoyl]-4-^{18}F-fluorobenzyl-L-cysteine (^{18}F-DCFBC), demonstrated feasibility and potential to detect metastatic prostate cancer with a radiation dose comparable to that of ^{18}F-FDG in the first human study (*2*). However, ^{18}F-DCFBC has high affinity for plasma protein, which produces slow clearance kinetics and high blood-pool activity that can interfere with the detection of lower avidity or smaller tumors (*3,4*). In contrast, 2-(3-{1-carboxy-5-[(6-^{18}F-fluoro-pyridine-3-carbonyl)-amino]-pentyl}-ureido)-pentanedioic acid (^{18}F-DCFPyL) showed 5 times higher PSMA affinity, better tumor

Received Aug. 8, 2019; revision accepted Nov. 11, 2019.
For correspondence or reprints contact: Matthias Eiber, Klinikum rechts der Isar, Ismaninger Straße 22, 81675 Munich, Germany.
E-mail: matthias.eiber@tum.de
Published online Dec. 13, 2019.

uptake, and more rapid plasma clearance than ^{18}F-DCFBC, resulting in higher tumor-to-blood and tumor-to-background ratios and lower accumulation in the liver (*5*). However, considerable kidney and salivary gland uptake still persisted in PET/CT with ^{18}F-DCFPyL (*5*). Furthermore, neither ^{18}F-DCFBC nor ^{18}F-DCFPyL includes a chelator capable of use for theranostic applications. In this regard, novel ^{18}F-based PSMA ligands, such as ^{18}F-PSMA-1007, were designed to have a radiochemical structure similar to PSMA-617, since PSMA-617 is a commonly used PSMA ligand for radioligand therapy. ^{18}F-PSMA-1007 exhibits an excellent sensitivity for the detection of small metastatic lymph nodes and showed predominant hepatobiliary excretion with reduced urinary retention of the tracer in the first human study (*6*). However, favorable tumor-to-background ratios can be acquired only at late imaging time points, that is, 3 h after injection, as ^{18}F-PSMA-1007 shares the slower tracer kinetics of PSMA-617 (*6*).

Radiohybrid PSMA ligands (rhPSMA) make up a new class of theranostic PSMA-targeting agents that allow fast radiolabeling with ^{18}F and radiometals. ^{18}F-rhPSMA-7 is the lead compound of this class and can be produced in high quantities relatively easily. Here, we assessed the biodistribution and image quality of ^{18}F-rhPSMA-7 to determine the optimal imaging time point.

MATERIALS AND METHODS

Patients

In a first step, all patients with histopathologically proven prostate cancer who underwent a clinically indicated ^{18}F-rhPSMA-7 PET/CT scan between October 2017 and June 2018 were collected from the institution's database. The administered activity was based on the patient's body weight (~4 MBq/kg). On the basis of experience with other ^{18}F-labeled PSMA ligands, an uptake time window of 1–2.5 h was defined. The specific uptake time for each patient was dependent on the logistics of the PET unit.

In a second step, 202 patients (mean age, 72.5 y; range, 49–91 y) were retrospectively selected and sorted into groups according to administered activity and uptake time. Twelve groups with a maximum of 20 patients each were established on the basis of both administered activity (3 groups: low, 222–296 MBq; moderate, 297–370 MBq; and high, 371–444 MBq) and uptake time (4 groups: short, 50–70 min; intermediate, 71–90 min; long, 91–110 min; and extra long, ≥111 min). Patients were stratified into the groups based on prostate-specific antigen (PSA) value and indication, to adjust for similar tumor stages. These patients were injected with a mean ^{18}F-rhPSMA-7 activity of 330 MBq (range, 232–424 MBq). PET/CT scanning was started on average 85 min after injection of ^{18}F-rhPSMA-7 (range, 58–153 min).

Clinical indications for ^{18}F-rhPSMA-7 PET/CT scanning were tumor recurrence for 145 patients and primary staging for 57 patients. The mean PSA level at the time of PET/CT scanning was 11.6 ng/mL (range, 0.1–95.3 ng/mL). The primary therapy for tumor recurrence was radical prostatectomy in 129 patients and external-beam radiation therapy in 16 patients; 42 patients received androgen deprivation therapy at the time of the PSMA-ligand PET scan or within 6 mo beforehand.

All patients gave written informed consent for the procedure. All reported investigations were conducted in accordance with the Helsinki Declaration and with national regulations. The retrospective analysis was approved by the Local Ethics Committee (permit 290/18S). Administration of ^{18}F-rhPSMA-7 was in accordance with the German Medicinal Products Act (AMG §13 2b) and the responsible regulatory body (government of Oberbayern). Table 1 summarizes the administered activities, uptake times, and clinical indications for the patient population. Synthesis of ^{18}F-rhPSMA-7 was performed as described previously (*7*). The patients received an injection of 20 mg of furosemide at the time of tracer application. To avoid potential interference from tracer retention in the urinary bladder, all patients were asked to void immediately before the PET/CT acquisition.

PET/CT Imaging

PET/CT imaging was performed from the base of the skull to the mid thigh, using a Biograph mCT flow scanner (Siemens Medical Solutions). All PET scans were acquired in 3-dimensional mode with an acquisition time of 1.1 mm/s in continuous table movement (the

TABLE 1
Stratification of Patients into Different Groups Based on Administered Activity and Acquisition Time

	Dose		Time			Mean BW	PSA (ng/mL)		Tumor locations (*n*)				
Group	Subgroup	MBq	Subgroup	Min	*n*	(kg)	Mean	Range	Local/prostate	LN	Bone	Visceral	Total
1	Dose 1	222–296	Time 1	50–70	20	69.1	16.7	2.6–95.3	14	23	4	1	42
2	Dose 1	222–296	Time 2	71–90	20	72.0	12.2	1.9–64.9	16	9	13	0	38
3	Dose 1	222–296	Time 3	91–110	20	72.0	12.0	0.9–81.6	12	17	7	0	36
4	Dose 1	222–296	Time 4	≥111	5	69.8	4.1	0.2–16.6	3	2	5	0	10
5	Dose 2	297–370	Time 1	50–70	20	83.0	12.2	2.3–39.5	12	10	14	0	36
6	Dose 2	297–370	Time 2	71–90	20	83.2	11.2	2.2–38.0	14	15	6	0	35
7	Dose 2	297–370	Time 3	91–110	20	82.2	12.1	2.3–41.4	13	17	13	0	43
8	Dose 2	297–370	Time 4	≥111	14	80.5	9.9	0.2–44.1	10	10	1	0	21
9	Dose 3	371–444	Time 1	50–70	20	100.4	12.3	2.0–60.0	13	20	11	1	45
10	Dose 3	371–444	Time 2	71–90	20	98.5	12.7	2.0–77.5	13	25	5	0	43
11	Dose 3	371–444	Time 3	91–110	16	99.3	9.0	0.2–62.7	10	8	2	0	20
12	Dose 3	371–444	Time 4	≥111	7	102.3	2.7	0.4–521	3	0	5	0	8
Total					202	84.1	11.6*	0.1–95.3	133	156	86	2	377

*Mean PSA value from all patients.
BW = body weight; local = local recurrence; LN = lymph node.

equivalent of 2 min per bed position in traditional mode). The acquired PET data were corrected and reconstructed iteratively by an ordered-subsets expectation maximization algorithm (4 iterations, 8 subsets) followed by a postreconstruction smoothing gaussian filter (5 mm in full width at half maximum). A diagnostic CT scan (240 mAs, 120 kV, 5-mm slice thickness) was performed in the portal venous phase 80 s after the intravenous injection of an iodinated contrast agent (iomeprol [Iomeron 300; Bracco], at 1.5 mL/kg of body weight; maximum, 120 mL).

Image Analysis

All quantitative and qualitative analyses were performed using non–time-of-flight/non-True X (Siemens) PET datasets. Quantitative analyses were conducted using OsiriX MD (Pixmeo SARL) with reformation into axial, coronal, and sagittal views. For evaluation of the biodistribution, circular volumes of interest with diameters of 20–30 mm were placed over the normal organs: parotid gland, submandibular gland, mediastinal aortic arch (blood pool), lungs, liver, spleen, pancreas, duodenum, kidneys, bladder, sacral promontory, and gluteus maximus muscle (background). For evaluation of tumor lesions, circular volumes of interest with diameters of 15 mm were placed for 3 lesions per patient in decreasing order of the SUV_{max}. Volume-of-interest placement and image analyses were performed by a board-certified nuclear medicine physician. SUV_{max} and SUV_{mean} were measured. SUV_{mean} was calculated using an isocontour of 50% of the SUV_{max}. Organ- and tumor-to-background ratios for SUV and SUV_{max} were calculated.

Qualitative image analyses were performed by a different board-certified nuclear medicine physician who was masked to the injected activity and the uptake time. The overall image quality, nonspecific blood-pool activity, and background uptake in bone or marrow were evaluated using 3- or 4-point scales. Details on the grading system are presented in Table 2.

TABLE 2
Grading Systems for Qualitative Image Analyses

Parameter	Group	Characteristic
Overall image quality	1	Good
	2	Moderate
	3	Poor
	4	Noninterpretable
Nonspecific blood-pool activity	1	No
	2	Slight; mainly in central vessels
	3	Moderate; also, in peripheral vessels
Background uptake in bone/marrow	1	No
	2	Slight (≤gluteal muscle*)
	3	Moderate (>gluteal muscle*)
	4	Focal spots
Negative impact of biodistribution on clinical decision making		Yes
		No

*SUV of background compared with that of gluteal muscle.

Statistical Analysis

For the analyses of continuous variables, the Kolmogorov–Smirnov test was used to assess the normality of the distribution. A 1-way ANOVA test was applied to compare means among groups for the normal parameters. If the ANOVA *F* statistic was significant, a post hoc pairwise comparison using a *t* test was conducted with Bonferroni adjustment. Before the ANOVA test, A Levene test was performed to test the homogeneity of variances across groups. The Welch robust ANOVA *F* test was performed when violating the assumption of homogeneous variances, and the Tamhane T2 test was considered for the post hoc group comparisons. Likewise, the Kruskal–Wallis test was performed for the nonnormal parameters. If that test was significant, a Mann–Whitney *U* test was conducted with Bonferroni adjustment for the pairwise comparisons. In addition, to evaluate trends across groups on parameters of interest, a linear-contrast test was performed for the normal parameters and a Jonckheere–Terpstra test was conducted for the nonnormal parameters. Supplemental Figure 1 shows the workflow for these statistical analyses (supplemental materials are available at http://jnm.snmjournals.org).

For the analyses of ordinal variables, the χ^2 test or the Fisher exact test was adopted to compare differences among groups, and the Mantel–Haenszel test was added to identify linear association among variables.

Data are expressed as mean ± SD and percentages for continuous and categoric variables, respectively. All statistical analyses were performed using the SPSS Statistics (version 25; IBM Inc.) and R (version 3.5.2). *P* values of less than 0.05 were considered statistically significant.

RESULTS

Quantitative Biodistribution

The biodistribution of ^{18}F-rhPSMA-7 was similar to that of established PSMA ligands. High levels of radiotracer uptake were observed in the salivary glands, liver, spleen, duodenum, kidneys, and urinary bladder. In contrast, uptake in the background, mediastinal blood pool, and lungs was minimal. Tracer retention was relatively low in the bladder. Physiologic uptake in bones was also low compared with other normal organs. Figure 1 shows the maximum-intensity-projection image of a patient with a normal biodistribution for ^{18}F-rhPSMA-7. Figure 2 summarizes the SUV_{mean} and the SUV_{mean} ratio in normal organs.

Biodistribution among healthy organs varied slightly with administered activity and uptake time. Data for differences and trends of means are presented in Tables 3 and 4. Background uptake was low and relatively stable across all administered activities and uptake times. Background SUV_{mean} showed statistically significant trends toward an increase with increasing administered activity and a decrease with increasing uptake time. However, the absolute differences were low (Tables 3 and 4).

SUV_{mean} in the blood pool, lungs, kidneys, bladder, and bones revealed further significant trends for different activities and uptake times. With increasing administered activity, SUV_{mean} increased in these organs (Table 3). With increasing uptake time, SUV_{mean} decreased in the blood pool and lungs and increased in the kidneys, bladder, and bones (Table 4). Figure 3 summarizes the differences in means and trends for SUV_{mean} of the blood pool, bone, kidney, and bladder for different uptake times.

Quantitative Evaluation of Tumor Lesions

In 187 of 202 patients included in the analyses, 377 tumor lesions were present in the PET scan (Table 1). Of 2 visceral lesions, one

FIGURE 1. ^{18}F-rhPSMA7 biodistribution: maximum-intensity-projection image illustrating tracer accumulation in salivary glands, liver, spleen, pancreas, bowel, kidneys, and bladder at 1 h after injection. Focal uptake (arrow) near bladder indicates lesion in prostate.

was in the lung and the other in the right testicle. Because of the low number of visceral lesions, they were excluded from the final statistical analyses. Supplemental Table 1 summarizes SUV_{mean} for tumor lesions according to tumor location, administered activity, and uptake time. SUV_{mean} for tumor lesions showed no clear differences with respect to administered activity or uptake time. When bone lesions were compared with all other soft-tissue lesions, they showed a significantly higher SUV_{mean} (15.63 ± 14.15 vs. 10.58 ± 19.28, $P < 0.001$) and SUV_{mean} ratio (28.59 ± 24.24 vs. 19.93 ± 20.24, $P < 0.001$).

Qualitative Image Analyses

The qualitative image analyses showed different patterns according to the administered activity and uptake time. Data for differences and trends of means are presented in Table 5. The overall image quality was stable for the different uptake times. With increasing administered activity, a trend toward decreasing overall image quality was noted. For example, the percentage of imaging datasets rated best (rating 1) decreased ($P < 0.001$).

For all other qualitative image parameters, there were no notable variations across the range of administered activity. In contrast, a significant trend toward less nonspecific blood activity ($P = 0.014$) and higher uptake in the bone marrow ($P = 0.011$) was observed with increasing time. Although nonspecific blood-pool activity was less likely to appear after longer uptake times, focal background spots in bone marrow were more common. Consequently, despite a paucity of data, a negative impact of the biodistribution on clinical decision making was more often noted with increasing uptake time ($P = 0.019$).

DISCUSSION

In this retrospective study, we quantitatively evaluated the biodistribution and tumor uptake of the new PSMA-targeting PET tracer, ^{18}F-rhPSMA-7. In addition, we qualitatively evaluated different uptake times and injected activities to determine those most favorable to image quality.

First, as expected, we showed that the normal biodistribution of ^{18}F-rhPSMA-7 is similar to other that of PSMA ligands.^{18}F-rhPSMA-7 PET exhibited high uptake in normal organs such as salivary glands and kidneys and moderate uptake in liver, spleen, and duodenum. Minimal uptake was observed in background tissue, blood pool, and lungs. The biodistribution pattern of ^{18}F-rhPSMA-7 is in line with the known expression of PSMA/FOLH1 (*8–11*). Low uptake in the urinary bladder suggests clearance of ^{18}F-rhPSMA-7 via the renal system, compared with mainly the biliary tract for ^{18}F-PSMA1007 (*6*).

The kidneys and the urinary tract are important organs in the biodistribution of a novel PSMA ligand. There are known limitations with, for example, ^{68}Ga-PSMA-11 and ^{18}F-DCFPyL, which are excreted mainly via the urinary tract. This elimination route can hamper assessment of local tumor and locoregional lymph nodes and can even induce halo artifacts, deteriorating image quality (*12,13*). The uptake patterns of the kidneys and bladder suggest the urinary excretory route for ^{18}F-rhPSMA-7. The uptake level in the kidneys was highly variable, as seen for other PSMA ligands used in PET imaging. However, one of the major strengths of ^{18}F-rhPSMA-7 is that tracer retention in the bladder was relatively low in all time-groups and clearly lower than that for ^{68}Ga-PSMA-11 (*14*).

Of note, the urinary retention observed in our analyses might be influenced by the application of furosemide at the time of tracer injection. The diuretic effect of furosemide begins within 5 min after intravenous injection and then progressively dissipates after peaking within the first 1–2 h because the plasma half-life of

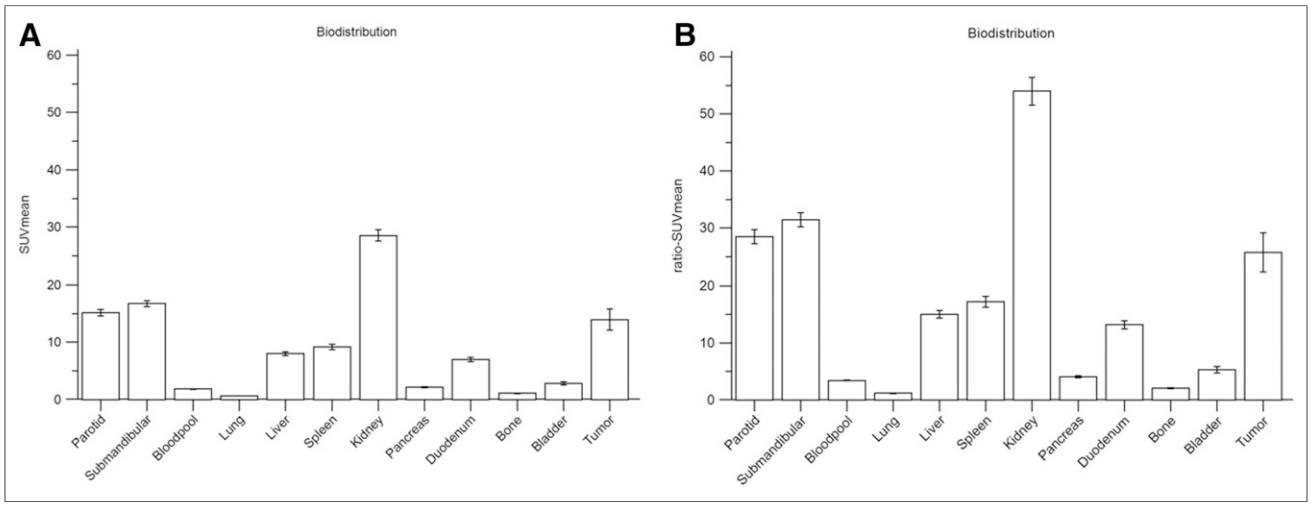

FIGURE 2. Bar graphs displaying normal distribution according to SUV_{mean} (A) and SUV_{mean} ratio (B). These graphs display biodistribution for entire patient cohort regardless of uptake time, and error bars show 95% confidence intervals for mean (data represent all patients analyzed, including all uptake times and administered activities).

TABLE 3
Quantitative Assessment of Biodistribution for Different Administered Activities

Organ	SUV_{mean}					SUV_{mean} ratio				
	Dose 1	Dose 2	Dose 3	P^1	P^2	Dose 1	Dose 2	Dose 3	P^1	P^2
Background	0.51 ± 0.07	0.55 ± 0.09	0.56 ± 0.07	<0.001*	<0.001*	—	—	—	—	—
Blood pool	1.74 ± 0.37	1.87 ± 0.42	2.00 ± 0.41	0.002	<0.001	3.42 ± 0.64	3.43 ± 0.77	3.57 ± 0.59	0.350*	0.200*
Lung	0.57 ± 0.15	0.64 ± 0.14	0.72 ± 0.12	<0.001*	<0.001*	1.12 ± 0.30	1.17 ± 0.24	1.29 ± 0.24	<0.001	<0.001
Kidney	25.50 ± 5.76	28.95 ± 7.55	31.31 ± 7.87	<0.001	<0.001	51.49 ± 16.17	53.61 ± 18.22	56.95 ± 17.40	0.200	0.040
Bladder	2.40 ± 1.59	2.91 ± 1.94	3.18 ± 2.25	0.007	0.001	4.86 ± 4.19	5.40 ± 3.85	5.78 ± 4.44	0.122	0.021
Bone	1.07 ± 0.28	1.11 ± 0.29	1.18 ± 0.32	0.065	0.015	2.12 ± 0.61	2.05 ± 0.63	2.13 ± 0.67	0.529	0.494
Parotid	15.01 ± 4.19	16.43 ± 4.25	13.88 ± 4.00	0.001	0.046	29.82 ± 9.13	30.25 ± 8.84	25.17 ± 8.22	<0.001	0.001
SMG	16.29 ± 3.66	17.74 ± 4.22	16.01 ± 4.03	0.011	0.155	32.39 ± 8.23	32.77 ± 9.30	29.04 ± 8.66	0.007	0.007
Liver	7.87 ± 2.46	8.31 ± 2.62	7.88 ± 2.31	0.562	0.432	15.67 ± 5.35	15.26 ± 5.04	14.16 ± 4.11	0.360	0.090
Spleen	9.09 ± 3.85	9.20 ± 3.15	9.37 ± 3.39	0.641	0.179	17.95 ± 7.67	16.92 ± 6.06	16.89 ± 6.55	0.863	0.297
Duodenum	7.10 ± 2.57	7.29 ± 3.15	6.69 ± 2.15	0.754	0.286	14.05 ± 5.08	13.36 ± 5.92	12.10 ± 4.09	0.145	0.026
Pancreas	2.14 ± 0.63	2.29 ± 0.80	2.13 ± 0.66	0.666	0.403	4.25 ± 1.32	4.25 ± 1.80	3.81 ± 1.20	0.073	0.014

*Normally distributed variable.
P^1 = group comparisons from ANOVA or Kruskal–Wallis test; P^2 = trend test from linear contrast test or Jonckheere–Terpstra test; SMG = submandibular gland.

furosemide is 1.5–2 h (*15,16*). The diuretic effect is reported to continue for up to 2 h after injection (*15*). Moreover, the individual bioavailability of furosemide varies considerably. In the present study, tracer retention in the bladder decreased with uptake time, and we did not observe a dose–response curve according to uptake time. However, to assess the specific excretion characteristics of the tracer, a comparison to patients without administration of furosemide would be necessary.

Assessing a new ^{18}F-labeled PSMA ligand requires determining the extent of background uptake in bone to limit false-positive findings and pitfalls (*17*). Bone uptake of ^{18}F-rhPSMA-7 is relatively low, at approximately half the level of the mediastinal blood pool. However, bone uptake increased with increasing uptake time, suggesting that ^{18}F-rhPSMA-7 accumulates in bone after specific binding. The etiology of this binding is still unknown, as PSMA expression is low in normal bone (*11*). Uptake in different bone pathologies (fractures, degenerative changes, fibroosseous lesions) has been reported to be related to PSMA expression in the neovasculature (*9*) and can be an issue for ^{18}F-labeled PSMA ligands, as recently reported (*18*). The qualitative analyses also indicate that imaging after a short versus long uptake time benefits bone uptake not related to prostate cancer, which can be a potential pitfall for image interpretation.

Tumor uptake of ^{18}F-rhPSMA-7 was in high ranges similar to those reported for other PSMA ligands, especially ^{68}Ga-PSMA-11 (*14,19*). Tumor uptake was also highly variable but without significant differences across tumor locations. However, tumor localization was easily achievable with the ^{18}F-rhPSMA-7 scan. Most tumor lesions were in the pelvis, and the average uptake of tumor lesions was sufficiently high to be distinguishable from the adjacent normal organs. In addition, as known for ^{68}Ga-PSMA-11, bone lesions showed a significantly higher uptake of ^{18}F-rhPSMA-7 than did soft-tissue lesions (*19*). No clear trend or significant differences were observed for tumor lesions across the various uptake times and administered-activity groups. Despite limitations due to the known high variation in PSMA expression in tumor lesions, these results indicate that uptake in tumor lesions is not a crucial determinant of optimal uptake time.

The qualitative image analyses revealed ^{18}F-rhPSMA-7 to have promising properties for prostate cancer imaging and provided useful data to inform decisions on optimal uptake time. In general, overall image quality was rated as high and stable across different uptake times. Whereas longer uptake times reduced nonspecific uptake in the blood pool, background uptake or focal spots in the bone marrow were seen to increase. Despite low absolute numbers, a negative impact of the biodistribution on clinical decision making was observed at later time points. Because blood-pool activity is not particularly relevant for prostate cancer image assessment and bone is a major site of metastases, qualitative analyses suggest an early time (~1 h after injection) as favorable for interpretation.

Regarding injected activity, our results indicate that overall image quality deteriorates with increasing administered activity. However, it is difficult to draw definitive conclusion, because our analysis found a clear correlation between patients' body weight and administered activity. It is known that image quality in PET worsens with increasing body weight. Qualitative assessment of nonspecific blood-pool and bone uptake was not dependent on body weight.

The optimal imaging protocol for PSMA-ligand PET requires further investigation, particularly the optimal time point. Various factors, such as the kinetics of radiopharmaceuticals, the physical characteristics of radioisotopes, and the purpose of the imaging, will all likely have an impact. Imaging time point varies from early dynamic imaging to 3 h after injection for ^{68}Ga-PSMA-11 PET (*20–24*). Some have advocated late imaging time points for PSMA-ligand PET; late imaging could be advantageous in detecting tumor lesions and getting a clear image mainly because of the increasing uptake of PSMA ligands over time (*14,22,25–27*). The preference for a late imaging time point seems to be in line with ^{18}F-based PSMA ligands; for example, imaging time points ranged from 1 to 3 h after injection for ^{18}F-PSMA-1007 (*6,28–30*). In a recent study comparing the biodistribution and tumor detection at 60 and 120 min after injection of ^{18}F-PSMA-1007, late imaging at 120 min after injection was recommended since lesions showed significantly higher uptake and better contrast (*30*).

TABLE 4
Quantitative Assessment of Biodistribution for Different Uptake Times

Organ	SUV_{mean}						SUV_{mean} ratio					
	Time 1	Time 2	Time 3	Time 4	P^1	P^2	Time 1	Time 2	Time 3	Time 4	P^1	P^2
Background	0.57 ± 0.07	0.54 ± 0.09	0.53 ± 0.06	0.53 ± 0.09	0.017*	0.006*	—	—	—	—	—	—
Blood pool	2.01 ± 0.45	1.90 ± 0.37	1.81 ± 0.40	1.63 ± 0.32	<0.001	<0.001	3.54 ± 0.72	3.56 ± 0.54	3.48 ± 0.79	3.09 ± 0.48	0.001†	0.015†
Lung	0.68 ± 0.16	0.64 ± 0.15	0.64 ± 0.14	0.57 ± 0.11	0.020*	0.005*	1.20 ± 0.29	1.21 ± 0.24	1.22 ± 0.28	1.10 ± 0.28	0.091	0.153
Kidney	26.81 ± 6.76	29.08 ± 7.37	29.21 ± 7.39	30.13 ± 9.01	0.093	0.008	48.09 ± 14.63	55.80 ± 17.17	55.98 ± 16.53	58.95 ± 22.37	0.010	0.001
Bladder	2.25 ± 1.28	2.84 ± 2.29	2.80 ± 1.42	4.22 ± 2.71	<0.001	<0.001	3.94 ± 2.16	5.48 ± 5.22	5.38 ± 2.79	8.22 ± 5.71	<0.001	<0.001
Bone	1.06 ± 0.27	1.12 ± 0.27	1.13 ± 0.28	1.20 ± 0.43	0.322	0.052	1.90 ± 0.51	2.12 ± 0.55	2.17 ± 0.59	2.34 ± 0.10	0.043	0.004
Parotid	15.21 ± 3.66	14.50 ± 4.72	15.05 ± 4.12	16.94 ± 4.52	0.048	0.108	27.10 ± 7.41	27.65 ± 10.19	28.94 ± 8.23	32.87 ± 10.07	0.012	0.003
SMG^+	16.31 ± 3.16	16.28 ± 3.70	16.75 ± 4.86	18.71 ± 4.32	0.048	0.031	29.16 ± 7.28	30.96 ± 8.23	32.32 ± 9.93	36.20 ± 9.71	0.006	<0.001
Liver	8.50 ± 2.30	7.94 ± 2.28	8.29 ± 2.75	6.60 ± 2.18	0.007	0.005	15.13 ± 4.38	15.09 ± 4.74	15.92 ± 5.38	12.87 ± 4.86	0.090	0.204
Spleen	9.67 ± 3.77	8.70 ± 3.10	9.47 ± 3.56	8.84 ± 3.12	0.476	0.313	17.30 ± 7.35	16.38 ± 5.78	18.21 ± 7.27	16.99 ± 6.26	0.525	0.176
Duodenum	7.20 ± 2.46	6.47 ± 2.27	7.37 ± 2.92	7.31 ± 3.39	0.293	0.498	12.86 ± 4.59	12.28 ± 4.50	14.20 ± 5.89	13.91 ± 6.03	0.384	0.167
Pancreas	2.403 ± 0.85	2.09 ± 0.53	2.13 ± 0.75	2.07 ± 0.57	0.094	0.014	4.31 ± 1.68	3.99 ± 1.21	4.09 ± 1.58	3.99 ± 1.46	0.742	0.148

*Normally distributed variable.
†Unequal variances across group.
P^1 = group comparisons from ANOVA, Welch ANOVA, or Kruskal–Wallis test; P^2 = trend test from linear contrast test or Jonckheere–Terpstra test; SMG = submandibular gland.

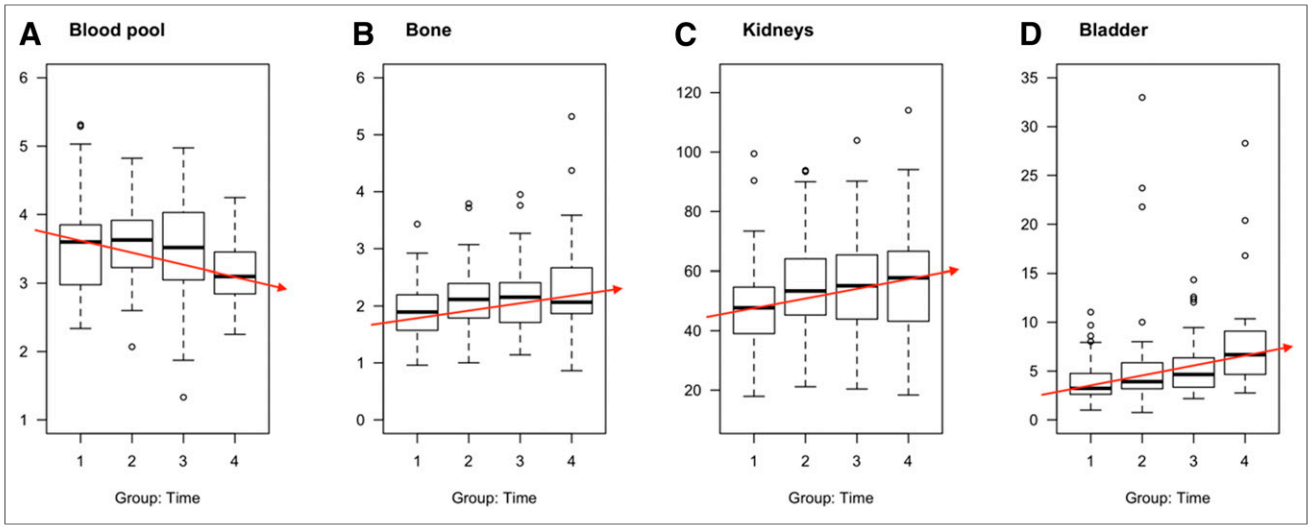

FIGURE 3. Changes in SUV_{mean} ratio according to uptake time. Increase in uptake time leads to decrease in retention in blood pool but increase in accumulation in normal bone, kidneys, and urinary bladder. *x*-axis gives different uptake time groups (group 1, 50–70 min; group 2, 71–90 min; group 3, 91–110 min; group 4, ≥ 111 min). A, C, and D show significant trends; B (bone) has *P* value of 0.052.

However, some have suggested that an early imaging time provides high enough diagnostic sensitivity. In a study comparing the diagnostic performance of ^{68}Ga-PSMA-11 PET at 1 h and 3 h after injection, early imaging at 1 h provided high image quality for detection of suspected prostate cancer lesions, with late imaging at 3 h potentially providing additional information to allow better interpretation of unclear lesions (*22*). Late imaging could offer the benefit of a high-contrast image, but without improving overall detection rates. Our study yields results similar to previous studies. Later imaging could be helpful to acquire clear images because of less nonspecific background activity; however, the overall image quality was stable over the imaging time points investigated. The impact on clinical decision making was negative at later imaging times. Thus, we recommended early imaging time points for ^{18}F-rhPSMA-7 to achieve the highest overall image quality.

Limitations of our study stem from its retrospective nature. Matched pairwise comparisons were unavailable, because PET imaging times and injected activities of ^{18}F-rhPSMA-7 were heterogeneous. To reduce heterogeneity among patients, we based the groups on imaging time and injected activity, and we performed groupwise analyses. However, for the patient collective available for this analysis, fewer than 10 patients could be included in groups 4 and 12. This low number of patients could also be a potential bias for the statistical analyses. Nevertheless, because we already see a trend toward a favorable uptake time of around 1 h, we believe that the potential bias is limited. In addition, we aimed for groups with homogeneous disease by stratifying on the basis of disease state and PSA value. However, it is known that substantial differences in tumor burden can be present in different patients with the same PSA level. Lastly, our study is not a substitute for a kinetic biodistribution study, since we retrospectively analyzed data acquired in routine clinical

TABLE 5
Qualitative Analyses of Image Quality

Parameter	Group	Dose 1	Dose 2	Dose 3	*P*	Time 1	Time 2	Time 3	Time 4	*P*
Overall subjective	1	37 (56.9%)	27 (36.5%)	11 (17.5%)	<0.001(F)	30 (50.0%)	17 (28.3%)	19 (33.9%)	9 (34.6%)	0.069 (F)
	2	28 (43.1%)	39 (52.7%)	45 (71.4%)	<0.001	27 (45.0%)	39 (65.0%)	34 (60.7%)	12 (46.2%)	0.063
	3	0 (0.0%)	8 (10.8%)	7 (11.1%)		3 (5.0%)	4 (6.7%)	3 (5.4%)	5 (19.2%)	
	4	0 (0.0%)	0 (0.0%)	0 (0.0%)		0 (0.0%)	0 (0.0%)	0 (0.0%)	0 (0.0%)	
Nonspecific activity in blood pool	1	11 (16.9%)	5 (6.8%)	3 (4.8%)	0.131 (C)	2 (3.3%)	5 (8.3%)	6 (10.7%)	6 (23.1%)	0.021 (F)
	2	9 (13.9%)	12 (16.2%)	13 (20.6%)	0.319	11 (18.3%)	7 (11.7%)	8 (14.3%)	8 (30.8%)	0.014
	3	45 (69.2%)	57 (77.0%)	47 (74.6%)		47 (78.3%)	48 (80.0%)	42 (75.0%)	12 (46.2%)	
Bone/marrow	2	44 (67.7%)	51 (68.9%)	44 (69.8%)	0.641 (F)	47 (78.3%)	42 (70.0%)	36 (64.3%)	14 (53.8%)	0.026 (F)
	3	20 (30.8%)	19 (25.7%)	15 (23.8%)	0.947	12 (20.0%)	16 (26.7%)	19 (33.9%)	7 (26.9%)	0.011
	4	1 (1.5%)	4 (5.4%)	4 (6.4%)		1 (1.7%)	2 (3.3%)	1 (1.8%)	5 (19.2%)	
Impact	Yes	2 (3.1%)	1 (1.4%)	4 (6.3%)	0.264 (F)	0 (0.0%)	1 (1.7%)	4 (7.1%)	2 (7.7%)	0.051 (F)
	No	63 (96.9%)	73 (98.6%)	59 (93.7%)	0.391	60 (100%)	59 (98.3%)	52 (92.9%)	24 (92.3%)	0.019

F = Fischer exact test and C = χ^2 test; otherwise, *P* value is for Mantel-Haenszel test.

care. Within this context, it needs to be stated that despite the low urinary retention observed in our patient cohort after the routine application of furosemide, the exact kinetics of tracer excretion have not yet been explored. An ongoing phase I study is currently investigating the biodistribution of ^{18}F-rhPSMA7.3 (NCT03995888).

CONCLUSION

The biodistribution of ^{18}F-rhPSMA-7 was similar to that of other established PSMA ligands with high image quality. The tumor uptake of ^{18}F-rhPSMA-7 was stable across the administered activities and uptake times. Because low tracer retention in the urinary bladder and the presence of focal uptake in the bone marrow are important features for PSMA-ligand PET imaging, early imaging time points (50–70 min) are recommended for ^{18}F-rhPSMA-7 to optimize image quality.

DISCLOSURE

Hans-Jürgen Wester, Alexander Wurzer, and Matthias Eiber are named as inventors on a patent application for rhPSMA. Hans-Jürgen Wester and Matthias Eiber received funding from the SFB 824 (DFG Sonderforschungsbereich 824, project B11) from the Deutsche Forschungsgemeinschaft, Bonn, Germany, and from Blue Earth Diagnostics Ltd. (licensee for rhPSMA) as part of an academic collaboration. Hans-Jürgen Wester is a founder, shareholder, and advisory board member of Scintomics GmbH, Fuerstenfeldbruck, Germany. Matthias Eiber and Wolfgang Weber are consultants for Blue Earth Diagnostics Ltd. No other potential conflict of interest relevant to this article was reported.

KEY POINTS

QUESTION: What imaging time for ^{18}F-rhPSMA-7 PET/CT achieves the highest overall image quality?

PERTINENT FINDINGS: The biodistribution of ^{18}F-rhPSMA-7 was similar to that of established PSMA ligands. Qualitative and quantitative analyses revealed increasing uptake in kidney, bladder, and bones over time and decreasing uptake in blood pool. Tumor uptake of ^{18}F-rhPSMA-7 was stable.

IMPLICATIONS FOR PATIENT CARE: These results suggest an early imaging time point (50–70 min) for ^{18}F-rhPSMA-7 PET/CT to achieve the highest overall image quality. Achieving the highest overall image quality could help patients by exact tumor localization and thus change patients' treatment strategies properly and efficiently.

REFERENCES

1. Sanchez-Crespo A. Comparison of gallium-68 and fluorine-18 imaging characteristics in positron emission tomography. *Appl Radiat Isot.* 2013;76:55–62.
2. Cho SY, Gage KL, Mease RC, et al. Biodistribution, tumor detection, and radiation dosimetry of ^{18}F-DCFBC, a low-molecular-weight inhibitor of prostate-specific membrane antigen, in patients with metastatic prostate cancer. *J Nucl Med.* 2012;53:1883–1891.
3. Rowe SP, Macura KJ, Mena E, et al. PSMA-based [^{18}F]DCFPyL PET/CT is superior to conventional imaging for lesion detection in patients with metastatic prostate cancer. *Mol Imaging Biol.* 2016;18:411–419.
4. Mease RC, Dusich CL, Foss CA, et al. N-[N-[(S)-1,3-dicarboxypropyl]carbamoyl]-4-[^{18}F]fluorobenzyl-L-cysteine, [^{18}F]DCFBC: a new imaging probe for prostate cancer. *Clin Cancer Res.* 2008;14:3036–3043.
5. Szabo Z, Mena E, Rowe SP, et al. Initial evaluation of [^{18}F]DCFPyL for prostate-specific membrane antigen (PSMA)-targeted PET imaging of prostate cancer. *Mol Imaging Biol.* 2015;17:565–574.
6. Giesel FL, Hadaschik B, Cardinale J, et al. F-18 labelled PSMA-1007: biodistribution, radiation dosimetry and histopathological validation of tumor lesions in prostate cancer patients. *Eur J Nucl Med Mol Imaging.* 2017;44:678–688.
7. Wurzer A, DiCarlo D, Schmidt A, et al. Radiohybrid ligands: a novel tracer concept exemplified by ^{18}F- or ^{68}Ga-labeled rhPSMA-inhibitors. *J Nucl Med.* December 20, 2019 [Epub ahead of print].
8. Israeli RS, Powell CT, Corr JG, Fair WR, Heston WD. Expression of the prostate-specific membrane antigen. *Cancer Res.* 1994;54:1807–1811.
9. Silver DA, Pellicer I, Fair WR, Heston WD, Cordon-Cardo C. Prostate-specific membrane antigen expression in normal and malignant human tissues. *Clin Cancer Res.* 1997;3:81–85.
10. Chang SS. Overview of prostate-specific membrane antigen. *Rev Urol.* 2004;6(suppl 10):S13–S18.
11. FOLH1. Human protein atlas website. http://www.proteinatlas.org/ENSG00000086205/normal. Accessed January 7, 2020.
12. Heußer T, Mann P, Rank CM, et al. Investigation of the halo-artifact in ^{68}Ga-PSMA-11-PET/MRI. *PLoS One.* 2017;12:e0183329.
13. Afshar-Oromieh A, Wolf M, Haberkorn U, et al. Effects of arm truncation on the appearance of the halo artifact in ^{68}Ga-PSMA-11 (HBED-CC) PET/MRI. *Eur J Nucl Med Mol Imaging.* 2017;44:1636–1646.
14. Afshar-Oromieh A, Malcher A, Eder M, et al. PET imaging with a [^{68}Ga]gallium-labelled PSMA ligand for the diagnosis of prostate cancer: biodistribution in humans and first evaluation of tumour lesions. *Eur J Nucl Med Mol Imaging.* 2013;40:486–495.
15. Wilcox CS, Mitch WE, Kelly RA, et al. Response of the kidney to furosemide. I. Effects of salt intake and renal compensation. *J Lab Clin Med.* 1983;102:450–458.
16. Brater DC. Diuretic therapy. *N Engl J Med.* 1998;339:387–395.
17. Sheikhbahaei S, Afshar-Oromieh A, Eiber M, et al. Pearls and pitfalls in clinical interpretation of prostate-specific membrane antigen (PSMA)-targeted PET imaging. *Eur J Nucl Med Mol Imaging.* 2017;44:2117–2136.
18. Rauscher I, Krönke M, König M, et al. Matched-pair comparison of ^{68}Ga-PSMA-11 PET/CT and ^{18}F-PSMA-1007 PET/CT: frequency of pitfalls and detection efficacy in biochemical recurrence after radical prostatectomy. *J Nucl Med.* 2020;61:51–57.
19. Prasad V, Steffen IG, Diederichs G, Makowski MR, Wust P, Brenner W. Biodistribution of [^{68}Ga]PSMA-HBED-CC in patients with prostate cancer: characterization of uptake in normal organs and tumour lesions. *Mol Imaging Biol.* 2016;18:428–436.
20. Kabasakal L, Demirci E, Ocak M, et al. Evaluation of PSMA PET/CT imaging using a ^{68}Ga-HBED-CC ligand in patients with prostate cancer and the value of early pelvic imaging. *Nucl Med Commun.* 2015;36:582–587.
21. Fendler WP, Eiber M, Beheshti M, et al. ^{68}Ga-PSMA PET/CT: joint EANM and SNMMI procedure guideline for prostate cancer imaging: version 1.0. *Eur J Nucl Med Mol Imaging.* 2017;44:1014–1024.
22. Afshar-Oromieh A, Sattler LP, Mier W, et al. The clinical impact of additional late PET/CT imaging with ^{68}Ga-PSMA-11 (HBED-CC) in the diagnosis of prostate cancer. *J Nucl Med.* 2017;58:750–755.
23. Schmuck S, Mamach M, Wilke F, et al. Multiple time-point ^{68}Ga-PSMA I&T PET/CT for characterization of primary prostate cancer: value of early dynamic and delayed imaging. *Clin Nucl Med.* 2017;42:e286–e293.
24. Schmuck S, Nordlohne S, von Klot CA, et al. Comparison of standard and delayed imaging to improve the detection rate of [^{68}Ga]PSMA I&T PET/CT in patients with biochemical recurrence or prostate-specific antigen persistence after primary therapy for prostate cancer. *Eur J Nucl Med Mol Imaging.* 2017;44:960–968.
25. Herrmann K, Bluemel C, Weineisen M, et al. Biodistribution and radiation dosimetry for a probe targeting prostate-specific membrane antigen for imaging and therapy. *J Nucl Med.* 2015;56:855–861.
26. Afshar-Oromieh A, Hetzheim H, Kratochwil C, et al. The theranostic PSMA ligand PSMA-617 in the diagnosis of prostate cancer by PET/CT: biodistribution in humans, radiation dosimetry, and first evaluation of tumor lesions. *J Nucl Med.* 2015;56:1697–1705.
27. Afshar-Oromieh A, Hetzheim H, Kubler W, et al. Radiation dosimetry of ^{68}Ga-PSMA-11 (HBED-CC) and preliminary evaluation of optimal imaging timing. *Eur J Nucl Med Mol Imaging.* 2016;43:1611–1620.
28. Giesel FL, Will L, Lawal I, et al. Intraindividual comparison of ^{18}F-PSMA-1007 and ^{18}F-DCFPyL PET/CT in the prospective evaluation of patients with newly diagnosed prostate carcinoma: a pilot study. *J Nucl Med.* 2018;59:1076–1080.
29. Giesel FL, Knorr K, Spohn F, et al. Detection efficacy of ^{18}F-PSMA-1007 PET/CT in 251 patients with biochemical recurrence of prostate cancer after radical prostatectomy. *J Nucl Med.* 2019;60:362–368.
30. Rahbar K, Afshar-Oromieh A, Bogemann M, et al. ^{18}F-PSMA-1007 PET/CT at 60 and 120 minutes in patients with prostate cancer: biodistribution, tumour detection and activity kinetics. *Eur J Nucl Med Mol Imaging.* 2018;45:1329–1334.